Seismic Fragility of a Bridge on Liquefaction Susceptible Soil

Oh-Sung Kwon
Department of Civil, Architectural, and Environmental Engineering Missouri University of Science and Technology, U.S.A.

Anastasios Sextos
Civil Engineering Department, Aristotle University Thessaloniki, Greece

Amr Elnashai
Mid-American Earthquake Center, Civil and Environmental Engineering Department, University of Illinois at Urbana-Champaign, U.S.A.

ABSTRACT: The paper presents the development of fragility curves for a bridge supported on liquefiable soil layers. A refined computational scheme is implemented for this purpose involving both a three-dimensional inelastic multi-platform model and a simplified nonlinear model calibrated to results from the three-dimensional model. Artificial earthquake records with long and short source-to-site distances are used to account for input motion uncertainty. Both uniform and non-uniform soil conditions along the bridge length are assumed to investigate the effect of incoherent input ground motion. Global damage indices which account for different soil, foundation and superstructure failure modes are proposed. Assumptions are made to facilitate the analysis; these are not integral to the procedure and are amenable to improvements in future studies. The results of the study indicate that the inelastic dynamic response and the subsequent damage of a soil-structure interacting system may be significantly affected by soil liquefaction. Moreover, it is shown that the spatial extent of liquefaction is a parameter that has to be considered as a source of uncertainty in input ground motion.

1 INTRODUCTION

Seismic vulnerability of bridges is often described by fragility curves which express the conditional probability that a bridge will reach or exceed certain damage states when subjected to earthquake ground motion effects. The inelastic dynamic response of a structural system is strongly affected by the randomness of material properties such as concrete and steel, and by the uncertainties in the input ground motion. Recent research (Kwon and Elnashai, 2006) has emphasized that in most cases, uncertainties in ground motion have a far more significant effect on the seismic fragility curves of structures compared to the randomness in structural material. For bridges supported on liquefiable ground, the uncertainty in soil material properties as well as the distribution of these properties along the bridge length should be considered in seismic fragility analysis. The effect of liquefaction on fragility analysis has not quantified. This is primarily due to the theoretical complexity and computational demands associated with large bridges, this deflecting attention and resources away from inelastic soil analysis aspects. Consequently, the scope of this paper is to investigate the importance of considering the effect of soil liquefaction on the vulnerability analysis for bridges supported on saturated cohesionless soil layers with loose-to-moderate density. The structural system adopted was relatively simple in order to focus on the parameters affecting liquefaction, earthquake ground motion and their overall effect on bridge vulnerability.

To achieve the stated objective, the well-studied (Zhang and Makris, 2001; Kwon, 2007) Meloland Road Overcrossing (MRO) bridge is adopted for this study. The bridge was built in 1971 and is located over Interstate 8 approximately 0.5 km from the fault rupture of the 1979 Imperial Valley earthquake. The bridge consists of two spans of pre-stressed box-girder decks monolithically connected to the center pier. The abutments are placed on fill. Seven piles support each abutment. Each side of abutment has 5.9 m of wing-wall. The pier at the center of the bridge has a diameter of 1.5 m and a height of 7.9 m from the top of piles. A total of 18 longitudinal reinforcement bars are used in the pier, the foundations of which are supported on 25 timber piles of 0.32m diameter, all spaced at 0.91 m. The overall procedure of earthquake ground motion selection and generation, aspects of site response and liquefaction consideration, analysis environment, and vulnerability assessment is presented below. Results are presented for various combinations of damage indices aiming at describing the different damage conditions that the bridge is anticipated to suffer from during seismic excitation.

2 INPUT GROUND MOTIONS AND FE MODELS FOR THE BRIDGE SYSTEM

2.1 *Generation of artificial ground motions*

In order to account for the inherent uncertainty of earthquake ground motion, six levels of ground motion intensity are used for the fragility analysis, i.e., 0.05g, 0.1g, 0.2g, 0.3g, 0.4g, 0.5g, all assumed at the bedrock level. It is worth noting that in contrast to a typical vulnerability assessment process where surface ground motion is used, it is necessary to select (or generate) ground motions at the bedrock level in order to consider the effect of strain softening of soil layers under cyclic loading during seismic wave propagation. In total, 18 artificial records were generated at the bedrock level, corresponding to three surface wave Magnitudes - m_s – namely 6.0, 6.5 and 7.0. Records at the bedrock level were generated as white noise emanating from the earthquake source using Monte-Carlo simulations for stationary processes (Manolis et al., 2007) and were rendered non-stationary through use of time envelope functions. Records were filtered through a Kanai-Tajimi (KT) filter, a high-pass (HP) filter, and a low-pass (LP) filter. The Magnitude-dependent filter values were derived according to Papageorgiou and Aki (1983). Peak ground acceleration was correlated to white noise intensity S_0 according to Shinozuka (1987) and to distance R. The duration was also considered as a variable, according to the corresponding magnitude M and epicentral distance R. From the numerous definitions of strong ground motion duration, the 'significant duration' was adopted (Trifunac and Brady, 1975), appropriately modified by a factor of 1.3 in order to derive the total signal duration required for the modulating function. It is noted that despite of the convenience of the Kanai-Tajimi power spectrum, numerous researchers have stressed its inability to represent the high frequency content of near field motions. Nevertheless, the reason that it was adopted in the present study is that, it provides an incremental level of earthquake intensity well controlled by the user. Therefore the target bedrock PGA of 0.05g, 0.1g, 0.2g, 0.3g, 0.4g and 0.5g is achieved in a smooth manner appropriate for fragility analysis. In order to account for the shortcoming in the representation of near-field motions, the frequency and damping of the HP filter were appropriately modified for all records assumed at distances R < 20km. A complete set of the Magnitude M and distance R values used can be found in Kwon et al. (2008).

2.2 *Selection of natural records*

As a means to complement the artificially-generated ground motions, it was deemed necessary to select an additional set of 18 records from a large database of available recordings (peer.berkeley.edu). Ground motions recorded at rock sites with PGA of 0.05g, 0.1g, 0.2g, 0.3g, 0.4g and 0.5g are selected. The selected ground motions are used as bedrock reference motion with minor scaling. Both near- and far-field records were sought in order to enrich the earthquake ground motion sample and further mitigate the inherent limitation of the artificial ground motions for near-field conditions due to the limitations of the Kanai-Tajimi spectrum. The catalogue of the ground motions used is presented in Kwon et al. (2008).

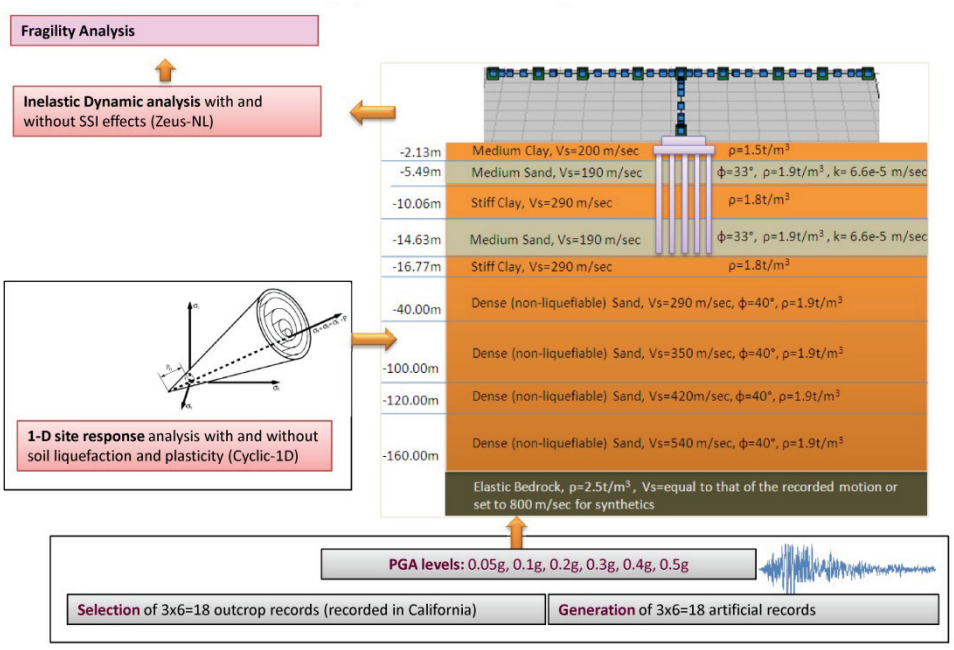

Figure 1: Overview of the fragility analysis scheme employed.

2.3 *Site response analysis considering liquefaction*

The selected ground motions were applied at the bedrock level and site response analysis was performed both with and without consideration of liquefaction effect. The bedrock was assumed elastic with shear wave properties corresponding to the rock conditions and water table was assumed at the ground surface. The soil column properties underneath the centre pier are illustrated in Figure 1. From the site response analyses with consideration of liquefaction effect, a significant reduction of the surface PGA was observed for moderate-to-high intensity bedrock motion. This was a consequence of the critical acceleration of the upper sand layers which was approximately 0.25-0.29 g (depending on the number of cycles). This acceleration 'cut-off' has resulted in the reduction of the imposed seismic demand at the base of the bridge compared to the case where liquefaction was not considered.

2.4 *Analysis Cases for SSI System*

Four analysis cases were considered with different assumptions in foundation and abutment representation. A set of reference analyses was performed corresponding to fully fixed support conditions and completely neglecting liquefaction and inelastic response of soil, thus corresponding to an essentially bridge analysis with fixed foundation (Case A). Next, the condition of nonlinear foundation and abutment compliance was considered based on the calibration with purely inelastic models presented below, but again neglecting the effect of soil liquefaction (Case B). This is essentially the case where both the superstructure and ground motion remain unchanged while the foundation conditions are represented by 6-DOF dynamic impedance matrices in the form of non-linear springs and dashpots. A more refined analysis considering the inelastic soil behavior was then performed using the multi-yield-surface plasticity model (Elgamal et al., 2002) incorporated into the computer program Cyclic-1D. The objective of this latter analysis was to provide a more refined surface input motion by considering soil liquefaction. In the computer code, the experimentally observed accumulation of permanent shear strain is modeled by using strain-space parameters and appropriate loading-unloading flow rules which are able to reproduce the dilation tendency and the resulting increase in cyclic shear stiffness and strength during earthquake loading. Indicative results of stress-strain response and pore water pressure build up are illustrated in Figures 2, 3 for the excitation case 1 (M=6.0, R=8.7kM, PGA=0.5g) where the liquefaction-induced flow of the sand layers has a significant effect on the resulting surface ground motion (Figure 3, left).

It is noted that the response at the soil surface was considered as the uniform earthquake foundation input motion for both bridge center pier and abutments (Case C). On the contrary the scenario that liquefaction occurs only below the center pier was also investigated (Case D), leading to asynchronous excitation of the bridge with support motions corresponding to the liquefaction susceptible soil profile at the center pier and the non-liquefiable, soil and embankment profile at the abutments. A summary of the analysis cases is given in Table 1.

Table 1Description of the analysis cases studied

Analysis Case	SSI	Liquefaction	Spatial variation of soil properties and motion
A	X	X	X
B	✓	X	X
C	✓	✓	X
D	✓	✓	✓

3 COMPUTATIONAL FRAMEWORK

Two different finite element models were assembled in order to achieve a balance between accuracy and computational efficiency for the vulnerability analysis. First, the concept of multi-platform simulation was employed using the pseudo-dynamic (PSD) simulation approach combined with sub-structuring. In this approach, a structure can be subdivided into several modules that are either physically tested or computationally simulated. UI-SimCor (Kwon et al., 2005), the program used in this analysis, was developed in order to coordinate analysis applications and/or hardware for structural testing and is described in detail in the given reference.

In the analysis of the MRO bridge, UI-SimCor was employed to enable the concurrent use of two different analysis packages and coordinated four distributed modules namely, (a) the bridge sub-system, which was modeled using the verified inelastic dynamic analysis platform ZEUS-NL (Elnashai et al., 2002), (b) the soil-pile foundation sub-system that was analyzed with OpenSees (McKenna and Fenves, 2001), as well as the left (c) and right (d), pile-supported, abutment-embankment system. The model was used to calibrate the center pier and abutment foundation stiffness of a second, simplified MRO bridge modeled in Zeus-NL (Kwon et al., 2008).

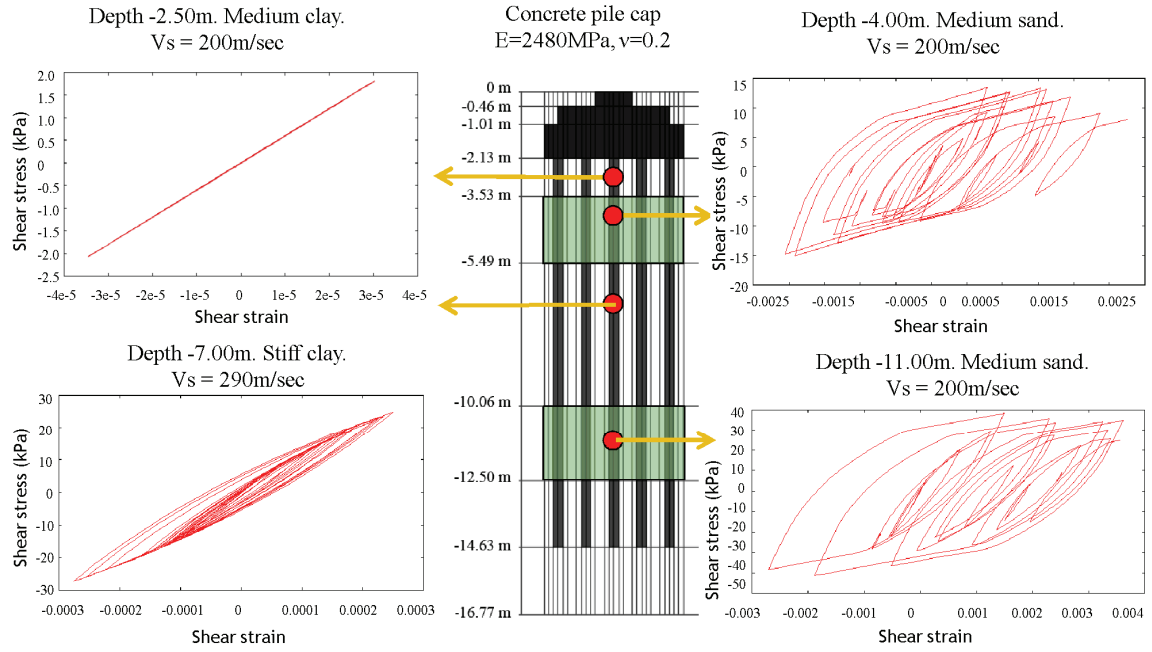

Figure 2: Stress-strain response of different soil layers

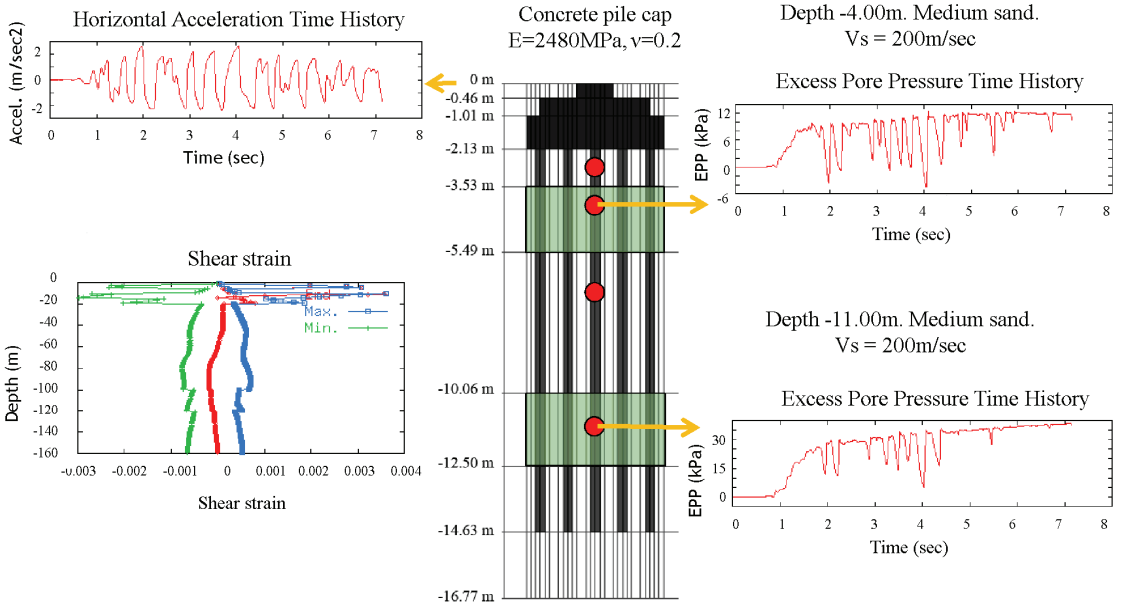

Figure 3: Build up of pore water pressure (right) and shear strain distribution with depth together with horizontal acceleration time history at the soil surface (left)

4 FRAGILITY ANALYSIS

4.1 *Procedure*

With the complete set of ground motions and calibrated inelastic finite element models, a total of 144 analyses were carried out. These comprise 4 different representations of the bridge system subjected to 36 ground motions. It was initially assumed that damage to the bridge occurs only at the bottom of the pier. Hence damage of an element corresponds to damage of the system. In Section 5, new damage indices are introduced to take account of excessive foundation lateral displacement, rotation as well as potential pile damage at the interface between liquefiable and non-liquefiable layers. The structural damage index, herein denoted as SDI to be distinguished from ground-related Damage Indices, for a pier was computed based on the Moment-Curvature relationship from response history analysis of the bridge system and the modified Park-Ang relationship (Kunnath et al., 1997):

$$SDI = \frac{\varphi_m - \varphi_y}{\varphi_u - \varphi_y} + \beta_e \frac{E}{M_y \varphi_u} \quad (1)$$

where φ_m is the maximum curvature achieved during cyclic loading, φ_y and M_y is the yield curvature and bending moment of the concrete section respectively, E is the cumulative energy absorbed in the hysteresis loops and β_e is a strength loss parameter set equal to 0.1.

After calculating the median DI values for each level of input intensity parameter (i.e. bedrock PGA), the Damage Index and Damage States were correlated according to Stone and Taylor (1993), i.e. damage limit state I ('repairable damage') was considered for values of 0.11<DI<0.40, damage limit state II ('irreparable damage') for values 0.40<DI<0.77 and damage limit state III ('collapse') for 0.77<DI<1.00. Four different fragility curves were then derived corresponding to the above four analysis cases and the probability of exceeding a particular level of damage d_{si} was calculated assuming lognormal distribution (a global factor of β_{dsi} = 0.6 was used to account for all sources of demand and supply uncertainty). As stated in the Abstract, the above assumptions with regard to the statistical model and the level of uncertainty are not hardwired to the framework presented in this paper.

4.2 *Comparative assessment of the effect of liquefaction on bridge fragility*

The resulting fragility relationships for each of the three aforementioned damage states are illustrated in Figure 4. It is observed that the introduction of soil-foundation compliance at the supports of the MRO Bridge has a less significant effect than liquefaction. Moreover, the probability of exceeding the 'repairable' damage limit state (I) is generally independent of the different representations of soil-foundation-structure system. This is primarily attributed to the fact that both soil-structure interaction and liquefaction are response aspects which become important at higher levels of ground excitation. Conversely, the 'irreparable' damage limit state requires significantly higher levels of earthquake intensity (as expressed in terms of bedrock PGA) in comparison with the cases of either local liquefaction or no liquefaction. The most important implication of spatially extensive liquefaction though, is that it essentially prevents the structure from reaching the critical 'collapse' limit state (III), since it reduces the imposed input accelerations to the level of the critical acceleration (0.25-0.29g). Consequently, the corresponding fragility curve for 'collapse' does not exist. Such reduction of earthquake forces due to liquefaction is indeed in agreement with a number of recent studies (e.g. Adalier and Elgamal, 2002). Another interesting aspect is the effect of the extent of liquefaction on the anticipated level of pier damage. As depicted in Figure 4, when liquefaction is localized below the Centre Pier, the flexural damage at the pier base was lower compared to the case where no liquefaction was considered, with all limitations presented above regarding the mechanisms considered, but clearly more critical than the 'global liquefaction' case. This increased seismic demand related to 'local liquefaction' is attributed to two main reasons:

(a) the abutments are subjected to acceleration higher than the critical acceleration of the liquefied ground below the center pier, hence, they essentially drive the motion of the bridge, while;

(b) the pier is subjected to additional pseudo-static forces arising from the considerable asynchronous seismic input, despite the short length of the bridge and the negligible phase lag of seismic waves.

5 PROPOSAL OF AN ALTERNATIVE DAMAGE INDEX

Based on the above observations and especially because liquefaction can reduce seismic demand to such an extent that the bridge does not reach collapse (Case C), it is important to recall that the fragility curves are inevitably related to the selected damage mechanisms, which were related solely to the flexural damage at the base of the center pier in this study. What is important to point out therefore is that despite the reduction of seismic demand in case of liquefaction, different and additional damage mechanisms could become relevant such as extensive rocking at the soil–pier foundation interface, damaging pile bending strains at the interfaces between soil layers of strong impedance contrast (i.e. successive liquefied and non-liquefied layers) and extensive movements at the abutments. The latter damage mechanisms are all not captured by the limit states adopted in the previous section. It is therefore interesting to investigate an additional global damage index accounting for the above liquefaction-induced mechanisms. Three additional failure modes and the corresponding damage indices are described below:

5.1 Lateral Soil Displacement Damage Index (LDI)

LDI represents structural damage due to the excessive soil movements at the foundation level that may lead to serviceability problems or instability of the superstructure. The LDI is derived based on the soil surface displacements as they are computed from site response analysis considering liquefaction. LDI and soil lateral displacements are correlated according to the values proposed by Bray and Stewart (2000) after appropriate modifications, as shown in Table 1. The assumption is made that the damage states described qualitatively by Bray and Stewart (2000) as 'zero', 'minor', 'moderate' and 'significant' damage correspond to the specific Damage Index values adopted herein for the pier damage (SDI), namely, 0, 0.11, 0.40 and 0.77. Moreover, a polynomial curve is fitted to allow continuous correlation between LDI and the computed maximum soil lateral displacements $u_{s,max}(t)$, i.e.:

$$LDI = 0.0004u_{s,max}^2\text{-}0.0416u_{s,max} + 0.0082 \quad (2)$$

It is also noted that the onset of Damage State I, 'Repairable damage', which essentially corresponds to the initiation of soil yielding, was set equal to 2.5cm after Park et al. (1994).

5.2 Foundation Rotation Damage Index (RDI)

The limit state RDI expresses the excessive pile group rotation that cause serviceability problems or instability of the superstructure. It is derived from the rotation of the foundation spring that is used in the finite element model to consider the compliance of the soil-pile group system. The rotational stiffness K_{xr} is computed with the use of the program ASING (Sextos et al., 2003) herein for the case of the 5x5 timber pile group of the MRO Bridge. It is noted that as the pile group dynamic stiffness is frequency-dependent, hence, the resulting stiffness is different for the 36 excitation cases studied (i.e. values for K_{xr} in the range of 80-130 kNm/rad are derived for dominant earthquake excitation frequencies between 1.8-3.0Hz). RDI and foundation rotation are correlated as previously stated from the values proposed by Bray and Stewart (2000) after appropriate modifications as summarized in Table 1. A polynomial curve is fitted to allow continuous correlation between RDI and the computed maximum foundation rotation $\theta_{,max}(t)$, given as:

$$RDI = 0.0276\,\theta_{max}^2\text{-}0.3456\,\theta_{max} + 0.0328 \quad (3)$$

5.3 Pile Bending Failure Damage Index (PDI)

PDI expresses the bending failure of the foundation piles at the interface between adjacent liquefiable and non-liquefiable layers. This is a well documented failure mode that has led the Japanese Highway code of practice (JRA, 1996) to advise practicing engineers to design piles against bending failure assuming that the non-liquefied crust offers passive earth pressure to the pile and the liquefied soil offers 30% of total overburden pressure. It is derived based on the magnitude of the soil surface displacements (conservatively assumed equal to those of the pile group top) as they are computed from site response analysis considering liquefaction and the displacement capacity Δ_{tp} of the timber piles given by the expression (ICC, 2007):

$$\Delta_{tp} = \frac{2\varepsilon_q L^2}{3D_p} \quad (4)$$

where L is the distance below ground to point of fixity (estimated to 8.0m), ε_q is the limiting strain values for timber equal to 4‰ and 8‰ for earthquake level 1 and 2 (corresponding to Damage States II and III since in contrast to RC members, a more flexible timber pile is considered as fully elastic up to strain level of 4‰) while D_p is the pile diameter equal to 0.32m.

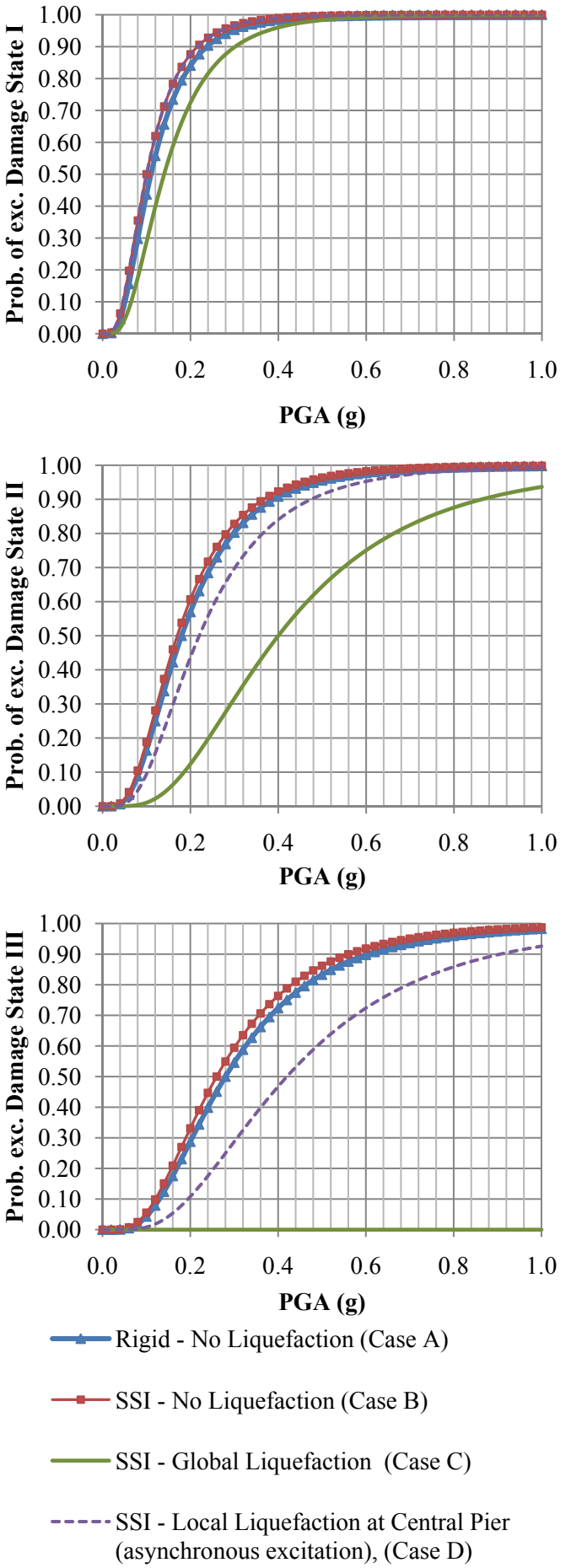

Figure 4. Fragility curves for the four foundation flexibility and excitation cases studied

From eq. (4) the displacement capacity of a timber pile is evaluated as 0.53m and 1.06m for Damage States II and III, respectively. It is noted that such high displacement capacity is in agreement with experimental studies reported in the literature (INA, 2001) where piles of similar diameter (i.e. 0.31m) where able to sustain deformation of up to 1m without experiencing significant damage. It is also noted that for the MRO Bridge studied, the limiting value of 0.53m was not exceeded, hence Damage State I was never reached (indicating fully elastic response) and PDI was set to zero for all 36 excitation cases. PDI and pile group top displacements are correlated using the values proposed in Table 2. Again, a polynomial curve is fitted to allow continuous correlation between PDI values and the computed maximum soil lateral displacements $u_{p,max}(t)$, that is (for $u_{p,max}(t)$ >0.53m):

$$PDI = 0.0002u_{p,max}^2\text{-}0.0447u_{p,max} + 1.5 \qquad (5)$$

Based on the above definitions, a Global Damage Index GDI_{sev} was then established expressing the severity of damage and determined from the maximum value amongst all the Damage considered above:

$$GDI_{sev} = \max\{SDI, LDI, RDI, PDI\} \qquad (6)$$

The resulting values of SDI, LDI, RDI and PDI for the 36 earthquake excitation cases studied are summarized in Table 2. It is observed in the table that for high values of bedrock PGA (i.e. PGA>0.3g) foundation displacement is the most critical in 44% of the cases studied, followed by structural damage (33%) and foundation rotation (22%). The fragility relationships for the case of Damage State III using the aforementioned alternative Local and Global Damage Indices are presented in Figure 5. It is seen that with the use of the GDI_{sev} definition, when ground and foundation damage is also considered, Damage State I ('repairable damage') is evident at significantly lower levels of excitation as a result of the early soil yielding compared to the case where only structural damage is accounted for (Figure 4). It is also noted that for the MRO Bridge studied the ultimate Damage State III was never reached even when the more refined Local Damage Indices that account for ground and foundation failure were implemented.

Table 2. Relation between Damage Indices and Damage States

Damage State	DI*	Lateral Displ. (cm)	Foundation Rotation (degrees)	Timber Pile Displ. (cm)
0 No damage	0.00	0	0	0
I Repairable	0.11	2.5	0.2	53.0
II Irrepairable	0.40	10.0	1.0	53.0
III Collapse	0.77	25.0	3.0	80.0
	1.00	40.0	4.0	106.0

* Damage Index refers to LDI, RDI and PDI for foundation displacements, rotation and pile top displacement respectively.

Table 3. Local and Global Damage Indices

PGA(g)	SDI	LDI	RDI	PDI	GDI_{sev}
0.50	0.35	0.16	**0.36**	0.00	0.36
0.40	0.32	0.15	**0.33**	0.00	0.33
0.30	**0.34**	0.12	0.30	0.00	0.34
0.20	0.20	0.11	**0.25**	0.00	0.25
0.10	0.10	0.09	**0.22**	0.00	0.22
0.05	0.00	0.06	**0.16**	0.00	0.16
0.50	**0.47**	0.45	0.40	0.00	0.47
0.40	**0.43**	0.40	0.39	0.00	0.43
0.30	**0.35**	0.33	0.34	0.00	0.35
0.20	0.23	**0.40**	0.29	0.00	0.40
0.10	0.09	0.21	**0.22**	0.00	0.22
0.05	0.00	0.13	**0.16**	0.00	0.16
0.50	0.51	**0.88**	0.40	0.00	0.88
0.40	0.45	**0.90**	0.39	0.00	0.90
0.30	0.37	**0.67**	0.34	0.00	0.67
0.20	0.24	**0.46**	0.29	0.00	0.46
0.10	0.06	**0.32**	0.20	0.00	0.32
0.05	0.02	0.14	**0.18**	0.00	0.18
0.50	0.49	**0.63**	0.40	0.00	0.63
0.40	0.35	**0.45**	0.30	0.00	0.45
0.30	**0.23**	0.17	0.23	0.00	0.23
0.20	0.01	0.03	**0.19**	0.00	0.19
0.10	0.00	0.02	**0.14**	0.00	0.14
0.05	0.00	**0.21**	0.14	0.00	0.21
0.50	0.26	**0.42**	0.32	0.00	0.42
0.40	**0.53**	0.24	0.39	0.00	0.53
0.30	0.14	0.05	**0.26**	0.00	0.26
0.20	0.17	0.24	**0.25**	0.00	0.25
0.10	0.00	0.06	**0.16**	0.00	0.16
0.05	0.00	0.11	**0.16**	0.00	0.16
0.50	0.29	**0.42**	0.32	0.00	0.42
0.40	0.39	**0.51**	0.35	0.00	0.51
0.30	0.07	0.09	**0.21**	0.00	0.21
0.20	0.08	0.09	**0.21**	0.00	0.21
0.10	0.11	0.15	**0.21**	0.00	0.21
0.05	0.00	0.09	**0.17**	0.00	0.17

* Bold indicates the most critical failure mode

This is true despite the increase in the GDI_{sev} values observed in Table 3. The latter observation is attributed to the acceleration 'cut-off' imposed by liquefaction. Conversely, at least from a qualitative point of view, it is seen in the same Table that liquefaction results to more extensive forms of damage (even if they are not substantially more severe), a fact that could not be observed without the implementation of the proposed local damage indices LDI, RDI and PDI.

6 CONCLUSSIONS

This paper reports an exploratory framework for including the effect of soil liquefaction in fragility analysis bridge-foundation-soil system. The framework is demonstrated through an application to the well-studied and instrumented Melloland Overcrossing Bridge. A powerful computational scheme was developed for this purpose involving both 3-D and simplified inelastic finite element models.

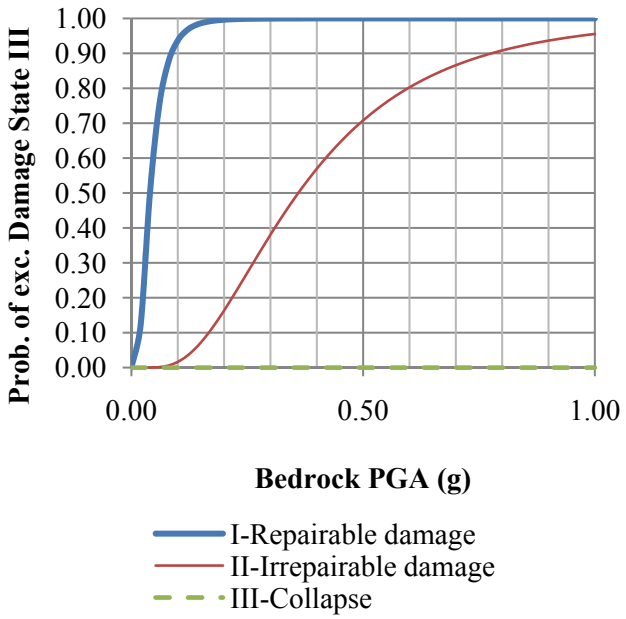

Figure 5. Fragility curves for the case of global liquefaction (CASE C) using an alternative Global Damage Index based on the severity of the overall damage.

Detailed inelastic site response analyses considering liquefaction effects were carried out. An effort is also made to propose a Global Damage Index accounting for different soil, foundation and superstructure failure modes. The results indicate that the inelastic dynamic response of the investigated bridge-foundation-soil system is significantly affected by the liquefaction of upper sand layers. In addition to the significance of accounting for liquefaction, the spatial extent of liquefaction is also shown to be important. Both liquefaction and its spatial distribution are influential on determining the characteristics of the input motion and the demand imposed on foundations and superstructure. The assumptions made to facilitate the application of the proposed framework for liquefaction-sensitive fragility analysis are not integral to the procedure and may be improved by researchers seeking to quantify the probabilistic response of soil-foundation-structure systems.

7 ACKNOWLEDGEMENTS

The contribution of the first author was sponsored by the Mid-America Earthquake Center, an NSF Engineering Research Center funded under grant reference EEC-9701785. The contribution of the third author was supported by the Federal Highway Administration, contract ref. ALTD3-1-080205-3.

8 REFERENCES

Adalier, K., and A.-W. Elgamal 2002. Seismic response of adjacent dense and loose saturated columns. *Soil Dyn. and Earthq.Eng.*, 22, 115-127.

Bray, J.D. and Stewart, J.P. 2000. Damage patterns and foundation performance in Adapazari, in Kocaeli, Turkey Earthquake of August 17, 1999 Reconnaissance Report. *Earthquake Spectra*, **16**(Suppl. A), 163–189.

Elgamal, A., Yang, Z. and Parra, E. 2002. Computational Modeling of Cyclic Mobility and Post-Liquefaction Site Response, *Soil Dyn. and Earthq. Eng.*, Vol. 22, No. 4, 259-271.

Elnashai, A. S., Papanikolaou, V., and Lee, D. 2002. Zeus NL – A System for Inelastic Analysis of Structures. *Mid-America Earthq. Center, University of Illinois at Urbana-Champaign.*

International Code Council 2007. California Building Code, Code of Regulations, Title 24, Part 2, Volume 2 of 2, U.S.

International Navigation Association 2001. Seismic Design Guidelines for Port Structures, Navigation Comm. WG 34.

Japanese Road Association 1996. Specification for Highway Bridges, Part V, Seismic Design.

Kwon, O.-S., Nakata, N., Elnashai, A. and Spencer, B. 2005. A Framework for Multi-Site Distributed Simulation and Application to Complex Structural Systems, *J. of Earthq. Eng.*, 9(5), 741-753.

Kwon, O.-S. Sextos, A and Elnashai, A. 2008. Liquefaction-dependent fragility relationships of complex bridge-foundation-soil systems', International Conf. on Earthquake Engineering and Disaster Mitigation, Jakarta, Indonesia.

Kwon, O.-S. 2007. Probabilistic Seismic Assessment of Structure, Foundation and Soil Interacting Systems, Ph.D. Thesis, University of Illinois at Urbana-Champaign.

Kunnath , S. El-Bahy, K., Taylor, A. and Stone, W. 1997. Cumulative Seismic Damage of Reinforced Concrete Bridge Piers, *NCEER Report 97/0006*, SUNY, Buffalo, N.Y.

Manolis, G.D, Rangelov, T.V. and Dineva, P.S. 2007. Free-field wave solutions in a half-plane exhibiting a special-type of continuous inhomogeneity, *Wave Motion* ,44(4), 304-321.

McKenna, F., and Fenves, G. L. 2001. The OpenSees command language manual, version 1.2., *Pacific Earthquake Engineering Research Center*, Univ. of California at Berkeley.

Papageorgiou, A.S. and Aki, K. 1983. A specific barrier model for the quantitative description of inhomogeneous faulting and the prediction of strong ground motion: I. Description of the model", *Bul. Seism. Soc. of America,* 73(3), 693-722.

Park, R. 1994. Comparative Bridge Examples, 2nd International Workshop on Seismic Design of Bridges, Queenstown ,New Zealand 1994, 2, 135-145.

Sextos, A., Pitilakis, K. and A. Kappos 2003. Inelastic dynamic analysis of RC bridges accounting for spatial variability of ground motion, site effects and soil-structure interaction phenomena. Part 1: Methodology and Analytical tools, Earthquake Engineering and Structural Dynamics, 32(4), 607-627.

Shinozuka, M. 1987. Stochastic fields and their digital simulation, in Stochastic Methods in Structural Dynamics, Martinus Nijhoff, Dordrecht, The Netherlands.

Stone, W. C. and Taylor, A.W. 1993. Seismic performance of circular bridge columns designed in accordance with AASHTO/CALTRANS standards, *NIST Building Science Series*, 170, Gaithersburg, M.D.

Zhang, J. and Makris, N. 2001. Seismic Response Analysis of Highway Overcrossings Including Soil-Structure Interaction, *PEER Research Report, 2001/02,* Berkeley, U.S.